MCT2 Overexpression Rescues Metabolic Vulnerability and Protects Retinal Ganglion Cells in Two Models of Glaucoma

Mohammad Harun-Or-Rashid[1],[*], Nathaniel Pappenhagen[2],[3],[*], Ryan Zubricky[2], Lucy Coughlin[2],[3], Assraa Hassan Jassim[2],[@], Denise M. Inman[2],[^]

[1]Case Western Reserve University, Cleveland, OH

[2]Department of Pharmaceutical Sciences, Northeast Ohio Medical University, Rootstown, OH

[3]School of Biomedical Sciences, Kent State University, Kent, OH

Abstract

Improving cellular access to energy substrates is one strategy to overcome observed declines in energy production and utilization in the aged and pathologic central nervous system. Monocarboxylate transporters (MCTs), the movers of lactate, pyruvate, and ketone bodies into or out of a cell, are significantly decreased in the DBA/2J mouse model of glaucoma. In order to confirm MCT decreases are disease-associated, we decreased MCT2 in the retinas of MCT2$^{fl/+}$ mice using an injection of AAV2-cre, observing significant decline in ATP production and visual evoked potential. Restoring MCT2 levels in retinal ganglion cells (RGCs) via intraocular injection of AAV2-GFP-MCT2 in two models of glaucoma, the DBA/2J (D2), and a magnetic bead model of ocular hypertension (OHT), preserved RGCs and their function. Viral-mediated overexpression of MCT2 increased RGC density and axon number, reduced energy imbalance, and increased mitochondrial function as measured by cytochrome c oxidase and succinate dehydrogenase activity in both models of glaucoma. Ocular hypertensive mice injected with AAV2:MCT2 had significantly greater P1 amplitude as measured by pattern electroretinogram than mice with OHT alone. These findings indicate overexpression of MCT2 improves energy homeostasis in the glaucomatous visual system, suggesting that expanding energy input options for cells is a viable option to combat neurodegeneration.

1. Introduction

Glaucoma is an optic nerve degeneration accompanied by vision loss believed to be a result of a progressive loss of retinal ganglion cell axons followed by their cell bodies (Buckingham et al., 2008; Howell et al., 2008). Indeed, it is this window between axonopathy and soma loss that may present a therapeutic window for glaucoma treatment (Crish et al., 2010). In the DBA/2J (D2) mouse model of glaucoma, optic nerves (ONs) are predisposed to neuropathy through metabolic deficiencies revealed through decreased resilience to oxygen-glucose deprivation (Baltan et al., 2010) and limits on metabolic switching when challenged (Jassim et al., 2019). Metabolic deficiencies in particular have shown promise as a potential target in the effort to reverse glaucoma (Harun-or-Rashid et al., 2018; Williams et al., 2017).

Glucose is the primary energy source for the mammalian brain (Siesjö, 1978), yet neurons can utilize lactate for oxidative metabolism. Astrocytes produce lactate as a glycolytic end-product which can be transported to neurons for use (Bouzier-Sore et al., 2006) via the monocarboxylate transporter (MCT) family (Halestrap, 2013a; Halestrap and Meredith, 2004; Simpson et al., 2007). A gradient of lactate in brain parenchyma enables lactate flux from astrocytes to neurons (Mächler et al., 2016). In locations such as the optic nerve, axons are provided this lactate from oligodendrocytes (Lee et al., 2012; Saab et al., 2016). Given the positioning of astrocytes between CNS vasculature and the nodes of Ranvier of ON axons (Dutta et al., 2018; Serwanski et al., 2017), it is possible that astrocytes are privy to axon energy needs and can supply glucose or lactate as well.

Within the MCT family, only MCT1 through 4 have been shown to transport monocarboxylates relevant to metabolism (Halestrap and Meredith, 2004). MCT1 is widely expressed early in postnatal development, and expression generally increases with age in astrocytes (Simpson et al., 2007). MCT2 is localized to neurons in the adult mouse brain and associated with the postsynaptic density protein PSD-95 (Pierre et al., 2002; Rafiki et al., 2003; Simpson et al., 2007). In the rat retina, MCT2 is heavily expressed throughout the inner retina, including the inner plexiform layer (Gerhart et al., 1999). Ancillary proteins such as basigin, embigin, and the neuroplastins Np55 and Np65 are necessary for MCT-1, −2, and −4 localization, chaperoning the transporters to the cell surface (Halestrap, 2013a; Wilson et al., 2013). MCT2 preferentially binds embigin (Halestrap, 2013b; Wilson et al., 2005). The chaperone proteins do not affect MCT lactate affinity (Ovens et al., 2010), but their association with the MCTs is necessary for maintaining activity (Manoharan et al., 2006). Of these four monocarboxylate transporters, our interest primarily lies with MCT2 because it is the main transporter for monocarboxylates to neurons. Inhibition of MCTs results in decreased retinal function with reductions in phototransduction sensitivity and reduction in neuronal levels of the neurotransmitter glutamate (B. V Bui et al., 2004). However, inhibition of MCTs caused no changes in retinal function when preceded by

ischemia (Melena et al., 2003). Ischemia/hypoxia leads to increases in glucose transporters (Yang et al., 2014), possibly decreasing the need for lactate transport, at least for fuel. Both MCT1 and MCT2 protein were significantly decreased in the D2 optic nerve despite stable axon number and glial hypertrophy (Harun-or-Rashid et al., 2018). It is thus hypothesized that MCT2 may be a therapeutic target where rescue of glaucomatous axons and protection of vision may be possible.

Monocarboxylate transporters, including MCT1 and MCT2, are upregulated in the D2 optic nerve after two months of the ketogenic diet (Harun-or-Rashid et al., 2018). A ketogenic diet is a low-carbohydrate, high-fat diet used to treat childhood epilepsies that are refractory to medication therapy. The ketogenic diet upregulated oxidative phosphorylation in mice, increased mitochondrial proteins and mitochondrial biogenesis, and elevated the phosphocreatine/creatine ratio (Bough et al., 2006; Harun-or-Rashid et al., 2018). This is consistent with studies that have shown that increases in lactate and the ketone body β-hydroxybutyrate are associated with increases in levels of MCT2 protein and mRNA (Takimoto and Hamada, 2014). This upregulation occurs at the level of translation through the stimulation of the PI3-kinase-AKT-mTOR -p70S6K pathway (Chenal et al., 2007; Harun-or-Rashid et al., 2018). MCT2 is the primary transporter for ketone bodies as well as lactate to neurons (Pierre et al., 2002; Simpson et al., 2007). As a result, it follows that the energy management of the neurons would be improved in glaucomatous conditions if more MCT2 were available. The question arises of whether the ketogenic diet is necessary or if upregulation of MCTs alone is sufficient to provide this protective effect for glaucoma.

We utilized adeno-associated virus (AAV-2) infection to increase MCT2 protein in two models of glaucoma, testing whether increasing MCT2 protein, and potentially monocarboxylate transport, could rescue metabolically challenged retinal ganglion cells (RGCs). We observed significant protection of RGCs and their axons, improved energy balance, mitochondrial function, and visual function after AAV2-directed MCT2 upregulation.

2. Materials and Methods

2.1 Animals

DBA/2J (D2), DBA/2J-Gpnmb+ (D2G), Tg(Thy1-cre/ERT2,-EYFP)HGfng/PyngJ (Thy1-cre) and B6.Cg-Gt(ROSA)26Sortm9(CAG-tdTomato)Hze/J (Rosa) mice were purchased from Jackson Laboratories (Bar Harbor, ME). MCT2$^{fl/fl}$ mice were a generous gift from Dr. David Gozal at the University of Chicago. All mice were bred and housed at Northeast Ohio Medical University. Both sexes of mice were used. The iris stroma, due to mutations in the *Tyrp1* and *Gpnmb* genes, atrophies in the D2 mouse, leading to blockage of the aqueous humor outflow pathways and development of glaucoma. In the D2G mouse, the wildtype *Gpnmb* allele ensures the pigment dispersion does not occur, so glaucoma does not develop (Howell et al., 2007). We crossed Thy1-cre and Rosa mice to generate progeny expressing tdTomato, a red fluorescent protein, in Thy1-positive cells, using these mice for our model of ocular hypertension. All procedures were performed in accordance with the National Institutes of Health guide for the care and use of Laboratory animals (NIH Publications No. 8023, revised 1978), with approval from the Institutional Animal Use and Care Committee.

2.2 Intraocular Pressure

A TonoLab rebound tonometer (Tiolat-Oy, Finland) calibrated for mice was used to measure intraocular pressure (IOP). Mice were lightly anesthetized with 2.5% isoflurane, then 10–20 measures from each eye were taken within 3 minutes to avoid any anesthetic-associated reduction of IOP. D2 mice had IOP measured at 10 months of age, then again at 12 months, prior to sacrifice. IOP measurements were taken prior to ocular hypertension (OHT) to establish a baseline IOP, then IOP was measured weekly after OHT. For IOP integral calculation, the difference between the baseline and weekly IOP was multiplied by the days between measurements then summed.

2.3 Diets

All mice, with the exception of a subset of 9-month-old D2 mice, were fed standard rodent chow (Formulab Diet 5008) *ad libitum*. The subset of D2 mice were fed a very low carbohydrate ketogenic diet (D12369B, Research Diets, New Brunswick, NJ) for 8 weeks. The standard diet was 26.8% protein, 56.4% carbohydrate, and 16.7% fat, while the ketogenic diet was 10.4% protein, 0.1% carbohydrate, and 89.5% fat. Mice undergoing diet transition were weighed prior to changing diets, then weekly while on the ketogenic diet. Food weight was also recorded to calculate consumption. Weights and food intake for mice on the ketogenic diet are in Table 1.

2.4 Virus

An AAV2.cre.GFP (1.0×10^{13} GC/mL; Vector Biolabs, Malvern, PA) was injected into MCT2$^{fl/fl}$ mouse eyes to remove the flox'd MCT2 gene through cre-mediated recombination, thereby eliminating MCT2 in the infected retinal cells. The AAV2 vector carrying MCT2, AAV2.CAG2.mSLC16A7–2A.eGFP, was also produced by Vector Biolabs. AAV2:MCT2 titer was 3.1×10^{12} GC/mL. The control virus, AAV2.CMV.PI.eGFP.WPRE.bGH, was produced by the University of Pennsylvania Penn Vector Core. AAV2:eGFP titer was 4.4×10^{12} GC/mL. Each injected eye received 2μL of virus.

2.5 Fundus Photography

The Micron IV (Phoenix Technology Group) system was used to image the fundus in experimental and control mice after AAV2 injection. Mice were anesthetized with a Ketamine (100mg/kg)-Xylazine (10mg/kg) cocktail, then given 0.5% Tropicamide (Henry Schein Animal Health) eyedrops to dilate the pupils. GenTeal eye lubricant (Alcon) was placed on each eye for imaging. Each viral vector carried an enhanced GFP reporter, so by imaging at 400nm excitation and 509nm emission, we were able to visualize AAV2-infected cells in the ganglion cell layer.

2.6 Vision Testing

The Diagnosys visual testing system (Celeris) was used to measure visual evoked potential and pattern electroretinogram. For both, mice were dark adapted for 1h, then anesthetized with Ketamine (100mg/kg)-Xylazine (10mg/kg) and placed prone on a heated stage. For visual evoked potential (VEP), Electrodes were placed in the mouse's cheek (reference),

scalp at the base of the skull, and the base of the tail (ground). Stimulators were placed on each eye and the output of 600 sweeps was processed to yield a waveform with two positive peaks (P1 and P2) and one negative peak (N1), from which a response amplitude was calculated (Absolute value of N1 + P2). For pattern electroretinogram (PERG), an integrated electrode and stimulator with moving bar was placed on either eye while the contralateral eye held an electrode measuring background activity. One hundred sweeps yielded waveforms with a negative peak (N1), a positive peak (P1) and a second negative (N2). We report P1 and N2 amplitude in μV.

2.7   Seahorse Analyzer

MCT2$^{fl/+}$ mice injected with AAV2-cre had their optic nerves removed and prepped for analysis in the Seahorse XF24 Analyzer as described (Jassim et al., 2019). The optic nerves were secured in an Islet capture microplate, within a plasma-thrombin clot, with DMEM (10mM glucose, 0.5mM sodium pyruvate, 4mM glutamine) as media. Optic nerves were subjected to the mitochondrial stress test (sequential addition of 10μg/mL oligomycin, 4μM FCCP, then 10μM antimycin-A), with either glucose or 2-deoxyglucose supplementation prior to oligomycin addition. The Analyzer measured oxygen consumption rate and extracellular acidification rate for each optic nerve.

2.8   Ocular Hypertension

Mice were anesthetized with isoflurane (2.5%), and 0.5% Tropicamide was placed on each cornea to dilate the pupils. Proparacaine hydrochloride (0.5%, Henry Schein Animal Health) was placed on the cornea after pupil dilation as a local anesthetic. Curved forceps were used to proptose and stabilize the eye while a glass pulled micropipette was used to inject 1.5μL of 8μL magnetic microbeads (UMC4F, Bangs Laboratories) into the central anterior chamber. Before the micropipette was removed, a neodymium magnet was used to pull the beads into the iridocorneal angle to occlude the trabecular meshwork. The micropipette was removed after the beads were distributed, and the mice were allowed to recover on a warm water blanket with Pura-Lube ophthalmic ointment on their eyes. There was no further use of the magnet after the initial injection. Two days after injection, IOP was measured as above and weekly thereafter for 4–5 weeks. Once the IOP integral reached 200mmHg-days, the mice were sacrificed, and tissue was analyzed.

2.9   Optic Nerve Analysis

Mice were given an overdose of sodium pentobarbital (300mg/kg, Beuthanasia-D). Optic nerves (ON) were removed and fixed by immersion in 2% paraformaldehyde with 2.5% glutaraldehyde in 0.1M sodium cacodylate buffer (pH 7.4). ON were stained with 2% osmium (Electron Microscopy Sciences), rinsed in sodium cacodylate, then taken through a series of graded ethanols to a 1:1 mixture of ethanol and propylene oxide, and finally, increasing concentrations of Ardalite 502/PolyBed® (02595–1, Polysciences, Inc) in propylene oxide. Nerves were incubated under vacuum in Ardalite 502/PolyBed® with three changes of embedding medium, until they were placed in a final embedding mold and cured in an oven for three days at 35, then 40, then 60°C. Embedded nerves were sectioned at 500nm using a Leica Ultramicrotome and a diamond knife (Diatom). Sections were mounted

on SuperFrost slides and stained with ρ-phenylenediamine (PPD). Axons were counted using unbiased stereology, described below.

2.10   Immunofluorescence and Microscopy

Immediately after sacrifice, eyes were removed and fixed in 4% paraformaldehyde for 30 minutes, then stored in 0.1M PBS. Retinas used for retinal ganglion cell (RGC) counting were dissected from the eye, cryoprotected in 30% sucrose with 0.02% sodium azide for 24 hours, and the vitreous was removed. Whole eyes, after cornea and lens removal, were embedded in OCT (Finetek, Fisher Scientific), sagittally sectioned at 10μm on a cryostat, and sections were placed on SuperFrost slides.

Immunolabeling for RBPMS, the RGC-specific antibody, commenced with 3 freeze-thaw cycles. All tissue was washed three times in 0.1M PBS, incubated in blocking solution (5% donkey serum, 1% Triton X-100 in 0.1M PBS) for one hour, incubated in primary antibody (diluted in blocking solution) for 18–72 hours, washed in PBS, incubated in secondary antibody (diluted in blocking solution), washed in PBS, then coverslipped with either Fluoromount-G or DAPI-Fluoromount-G (Southern Biotech). Primary antibodies and their concentrations are listed in Table 2. Secondary antibodies were from Jackson ImmunoResearch and included Alexa Fluor 488, 594, or 647 conjugated to anti-rabbit, anti-mouse, or anti-goat IgG.

Retinal sections immunolabeled with α-Rb MCT2 primary antibody were incubated with TrueBlack Lipofuscin Autofluorescence Quencher (Biotium) for thirty minutes after blocking and before primary antibody incubation, then washed three times with 0.1M PBS.

For microscopy, a Leica DMi8 confocal microscope (Leica Microsystems, Buffalo Grove, IL, USA) was used. Photomicrographs were captured with consistent exposure and laser intensities among groups. Quantification of Iba1 immunofluorescence was undertaken by measuring fluorescence intensity across microglial cell bodies within regions of interest (ROI) using Fiji-ImageJ. At least 12 ROIs were used per antigen for quantification.

For mitochondrial analysis, we used the particle size estimator (Fiji-ImageJ) on maximum intensity projections of confocal photomicrographs (n=12 images per stack) of the inner retina imaged using the Leica confocal at 63x. These data quantified particle number (in this case, Tom20-immunolabeled mitochondria) and estimated size. At least 12 image stacks per group were analyzed.

2.11   Cell and Axon Quantification

Whole mounted retinas immunolabeled with RBPMS and PPD-stained optic nerve (ON) sections were counted using the optical fractionator approach for unbiased stereology and either a 40x (retina) or 100x (ON) objective (StereoInvestigator software, MBF Bioscience). Between 35 and 40 sampling sites (3%) of each tissue were counted. The coefficient of error (Schmitz-Hof) was kept at 0.05 or below for all stereological counting, ensuring sufficient sampling rate. Iba1 density was calculated by manually counting Iba1-positive cell bodies in the inner retina using a 40x objective, then dividing by the area calculated within Stereoinvestigator. At least 6 sections per group were counted.

2.12 Hexokinase Activity

Optic nerves were isolated from sacrificed mice and flash frozen in liquid N_2. Hexokinase activity was quantified using a hexokinase assay kit (ScienCell), in accordance with the manufacturer's instructions. Assay results were normalized to the total protein level in each ON sample as quantified with the Pierce BCA protein assay kit (ThermoFisher Scientific).

2.13 SDH and COX Histochemistry

Freshly isolated optic nerves (ONs) were flash frozen in liquid N_2 and held at −80°C until embedding in OCT and sectioning on a cryostat. Control and experimental ONs were sectioned onto the same slide and enzymatically treated simultaneously. All chemicals for histochemistry were obtained from Sigma-Aldrich. ON sections were incubated in 1.5nM nitroblue tetrazolium (N6876), 130mM sodium succinate (S2378), 0.2mM phenazine methosulfate (P9625), and 1mM sodium azide in 0.1M PBS pH=7.0 for 40 min at 37°C for succinate dehydrogenase (SDH) histochemistry. ON sections for cytochrome-c oxidase (COX) were incubated with 1X diaminobenzidine (D4293), 100μM cytochrome c (D2506) and 4 IU/mL catalase (C9322) in 0.1M PBS pH=7.0 for 40min at 37°C. Slides were dehydrated through graded alcohols to xylenes then coverslipped with DPX mounting media.

2.14 Protein Analysis

Fresh or flash-frozen ONs were placed in T-PER buffer (Thermo Fisher Scientific) with HALT protease and phosphatase inhibitors (78442, Thermo Fisher Scientific) and homogenized with three 1s pulses at 10% amplitude using a Branson Sonicator. Lysates were centrifuged at 10,000g for 10 min at 4°C; supernatants were collected and used for protein quantification using capillary tube-based immunoassay in the Wes (ProteinSimple). Using the Wes, protein analysis was repeated three times using biological replicates. Wes results are normalized to total protein in the sample, as measured by capillary electrophoresis.

2.15 Experimental Design and Statistical Analysis

GraphPad Prism software (version 8.0) was used to generate statistics for quantitative data. Data were analyzed for normality before two-tailed t-test (normally distributed data), or with the non-parametric Mann-Whitney test (non-normally distributed data). One-way ANOVA and Tukey's multiple comparison post hoc test was used to compare multiple groups within a strain, or across multiple groups within an outcome measure. $P<0.05$ was considered statistically significant, and data are reported as mean±SD, unless otherwise noted.

3. Results

3.1 MCT2 Decrease Compromises Visual Function and ATP Production

MCT2 protein is significantly decreased in the glaucomatous retina and ON (Harun-or-Rashid et al., 2018). To evaluate the negative impact on mitochondrial bioenergetics of MCT2 loss, we injected MCT2$^{fl/+}$ mice with an AAV2-cre, generating mice with decreased MCT2 in retinal cells that were infected by the AAV2-cre-GFP. At one and two weeks post-

infection, we took fundus photographs to evaluate infection rate and progress. GFP-positive infected cells were observed throughout each injected eye, though the cells were brighter and more distinct at two weeks (Figure 1A). We measured visual evoked potential (VEP) in the mice to determine the functional impact of MCT2$^{fl/+}$. There was a significantly lower response amplitude (N1 trough to P2 peak) in the cre-induced MCT2$^{fl/+}$ mice compared to B6 control (p<0.01; Figure 1B). Representative VEP traces are shown in Figure 1C. The optic nerves from these mice were then evaluated in the Seahorse XF24 Analyzer for oxygen consumption rate (OCR) and extracellular acidification rate (ECAR). MCT2 haploinsufficiency resulted in significantly decreased oxygen consumption for the production of ATP in the cre-induced MCT2$^{fl/+}$ optic nerve (ON) compared to C57Bl/6 (B6) age-matched control, regardless of whether the ONs were in media supplemented with glucose (Glc) or 2-deoxyglucose (2-DG; Figure 1D). The OCR in the B6 ON with 2-DG was no different than when Glc was the substrate, suggesting that there was sufficient lactate or pyruvate stores in the B6 for the ONs to continue ATP production. The cre-induced MCT2$^{fl/+}$ ATP production with either 2-DG or Glc as substrate was no different from the other, but significantly lower than B6 ON, indicating MCT2 haploinsufficiency had a negative overall effect on OCR. In Figure 1E, the extracellular acidification rate (ECAR) was significantly lower in both B6 and MCT2$^{fl/+}$ ON with 2-DG as substrate, reflecting significantly reduced proton release from lactate production.

3.2 MCT2 Overexpression through AAV2:MCT2

Confirming a negative impact on VEP and ATP production with decreased MCT2, we then tested the hypothesis that providing greater access to energy substrates through the upregulation of MCT2 would preserve RGC function. We first immunolabeled control retina to demonstrate localization of MCT2 on RGCs (Figure 2A). The figure panels show retina immunolabeled with antibodies against MCT2, NeuN (neurons), and Vimentin (Müller glia). MCT2 immunolabel is found on RGCs (arrows) and Müller glia endfeet (arrowheads), as well as within the inner plexiform and inner nuclear layers (Figure 2A). In order to upregulate MCT2 in RGCs, we took advantage of the ability of AAV2 to infect neurons after intraocular injection. Figure 2B shows sectioned 12-month-old D2 retina (two months after AAV2:MCT2 injection) with RBPMS-positive RGCs (red), and AAV2:MCT2-positive cells (green from the eGFP reporter). The virus infected both RGCs and neurons in the ganglion cell layer (GCL) and inner nuclear layer (INL) that may be either displaced RGCs or amacrine cells. In some retinas (n=2 out of 25), photoreceptors were observed to be eGFP-positive (data not shown). Figure 2C is the fundus photograph from the AAV2:MCT2 infection in the 10.5-month-old D2 eye two weeks after injection. A further confirmation of the AAV2:MCT2 infection of RGCs is the virus eGFP reporter expression in axons of the optic nerve two months after injection (Figure 2D). Figure 2E shows the distribution of AAV2:MCT2-infected cells observed through the retina.

3.3 MCT2 Overexpression Protects RGCs from Degeneration

Mean D2 mouse IOP for all groups (untreated, AAV2 with or without ketogenic diet) at 10 months of age and prior to intervention was 21.7±0.75; at 12 months of age, prior to sacrifice, mean IOP was 22.5±0.9. There was no apparent impact on IOP of the AAV2:MCT2 injection. Treated D2 mice were injected with AAV2:MCT2 at 10 months of

age. As previous data in our laboratory demonstrated that placing D2 mice on a ketogenic diet for two months resulted in upregulation of MCT2, we sought to probe whether diet would be necessary for the function and maintenance of the MCT2 after viral-mediated overexpression. Therefore, we included an AAV2:MCT2 injected group of D2 mice also on the ketogenic diet. The AAV2:MCT2 injected eyes, regardless of diet, had significantly greater RGC density than the 12-month-old age-matched untreated D2 retina (Figure 3A, p<0.0001). Images of retinas immunolabeled with RBPMS for RGCs showed RGC loss in the untreated D2 retina (Figure 3B). Cross-sections of optic nerves stained with ρ-phenylenediamine (Figure 3C) show loss of axons in the untreated D2 and in the AAV2:MCT2 D2 mice on the ketogenic diet (KD). The AAV2:MCT2-injected D2 mice on a normal diet had significantly greater axon number in the optic nerve (ON) than untreated D2 (Figure 3D, p<0.0001). However, the 12-month-old D2 mice on the ketogenic diet showed significantly lower axon number than D2 mice on the control diet (p<0.05), despite a few animals with axon number in the normal range.

3.4 MCT2 Overexpression Increased Mitochondrial Activity

To confirm upregulation of MCT2 protein through viral-mediated overexpression, we used capillary electrophoresis to quantify MCT2 in the ON, finding MCT2 levels that matched the D2G mouse ON and were significantly greater than the untreated 12-month-old D2 ON (Figure 4A, p<0.0001). We evaluated whether MCT2 upregulation would have a compensatory effect on MCT1 expression, so we quantified MCT1 in the ON. MCT1 protein is significantly higher in D2G and D2 mice injected with AAV2:MCT2 than untreated D2 mice (Figure 4B, p<0.05). The ratio of phosphorylated AMP kinase (pAMPK) to AMP kinase increases when ATP levels are low. The D2 mice have significantly higher pAMPK/AMPK ratio in the ON than either the D2G control or the D2 injected with AAV2:MCT2 (Figure 4C, p<0.001). PGC-1α (PPARγ coactivator 1) stimulates mitochondrial biogenesis and plays a central role in cellular metabolism, so we anticipated it may be altered by MCT2 overexpression. PGC-1α protein in ON from D2 mice infected with AAV2:MCT2 is significantly increased compared to both untreated D2 and D2G mice (Figure 4D, p<0.01). Upregulation of MCT2 may impact the balance of energy derived from glycolysis versus oxidative phosphorylation, so we evaluated hexokinase activity, the first enzyme in the glycolytic pathway and a key regulator of glycolytic flux (Tanner et al., 2018). Hexokinase activity is upregulated in D2 mice injected with AAV2:MCT2 compared to untreated D2 mice (Figure 4E, p<0.05). Succinate dehydrogenase (SDH) activity, contributing to both the TCA cycle and the electron transport chain, can be a proxy for cellular respiration rate. We observed that SDH activity in ON cross-sections subjected to SDH histochemistry is significantly higher in D2G and D2 mice injected with AAV2:MCT2 than untreated D2 (Figure 4F, p<0.0001). Example cross-sections of ON with SDH histochemistry are shown in Figure 4G.

3.5 Microglial Activation Increased with AAV2:MCT2 Injection

Virus injection can induce an inflammatory response, so we evaluated microglia in the experimental retinas. Iba1-positive microglia are observed in all retinas, primarily in the outer plexiform, inner plexiform, and ganglion cell layers (Figure 5A–D). In the untreated 12 month-old D2 retina (Figure 5A), the Iba1-positive microglia are intensely labeled and

less ramified than the D2G control retinas (Figure 5B). Numbers of microglia and their Iba1 labeling intensity increase in both groups injected with AAV2:MCT2 (D2 mice ± ketogenic diet), Figure 5C and D. Both AAV2:MCT2 injected D2 ± ketogenic diet show significantly higher microglial density than untreated D2 and D2G mouse retina (Figure 5E, $p<0.0001$). Iba1 fluorescence intensity, correlated to the level of microglial activation (Bosco et al., 2008; Imai and Kohsaka, 2002; Ito et al., 1998), is highest in the AAV2:MCT2 injected D2 retina on the control diet. Untreated D2 retina has significantly higher Iba1 fluorescence intensity compared to untreated D2G mice (Figure 5F, $p<0.001$). D2 mice injected with AAV2:MCT2 ± the ketogenic diet have higher Iba1 activation than untreated D2 mice (Figure 5F, $p<0.05$ and $p<0.001$).

3.6 MCT2 Overexpression Rescued RGCs after Ocular Hypertension

To further explore the effects of increasing MCT2 expression in the context of glaucoma, we undertook an analysis of mice injected with AAV2:MCT2 after being subjected to ocular hypertension. Figure 6A shows flatmount retina from a Thy1-tdTomato mouse injected with AAV2:MCT2. There is widespread colocalization of Thy1-positive RGCs and the eGFP from the virus reporter. Figure 6B shows the intraocular pressure (IOP) profiles for the OHT groups: OHT with AAV2:MCT2 injection, OHT with control virus (AAV2:eGFP) injection, and OHT alone. All OHT groups underwent significant increases in IOP ($p<0.001$) compared to baseline values. Mice were held until each achieved 200mmHg-Days of IOP increase, hence the range in weeks of IOP measurement. There were no statistical differences across OHT groups for peak IOP or IOP integral. RGC density is significantly higher in OHT mice injected with AAV2:MCT2 and control mice than in OHT mice (Figure 6C, $p<0.01$). ON axon number is also significantly higher in OHT mice injected with AAV2:MCT2 and control mice than in OHT mice (Figure 6D, $p<0.001$, and $p<0.01$, respectively). OHT mice injected with AAV2:MCT2 have significantly higher MCT2 protein in retina than both control and OHT retina (Figure 6E, $p<0.001$ and $p<0.0001$). In ON, there is a significant effect of group on MCT2 protein, though no individual statistical differences were observed (ANOVA, $p<0.05$, Figure 6F).

3.7 MCT2 Overexpression Reduced Metabolic Stress after OHT

AAV2:MCT2 infection changes the metabolic activity in OHT mice. OHT mice injected with AAV2:MCT2 have a significantly lower pAMPK/AMPK ratio in ON than control mice, and OHT mice injected with AAV2:eGFP (Figure 7A; $p<0.01$, and $p<0.05$ respectively). PGC-1α protein in ON shows no change across control and experimental groups (Figure 7B). In contrast to the D2 experiments which showed significantly greater hexokinase activity with AAV2:MCT2 infection, hexokinase activity is significantly lower in OHT mice injected with AAV2:MCT2 compared to OHT alone (Figure 7C, $p<0.05$). Mitochondrial size is not different between OHT mice with either AAV2:eGFP or AAV2:MCT2 infection (Figure 7D).

3.8 MCT2 Overexpression Increased Mitochondrial Function after OHT

COX and SDH activity are significantly increased in OHT mice injected with AAV2:MCT2 compared to OHT alone. Lower COX activity in OHT control ON compared to the AAV2:MCT2 OHT group is evident in the high magnification insets of Figure 8A (compare

a' to b'). SDH is also less active in OHT mice (Figure 8C, c') than in OHT mice injected with AAV2:MCT2 (Figure 8D, d'). OHT mice injected with AAV2:MCT2 have significantly lower SDH activity than control mice (Figure 8E, $p < 0.001$), but significantly higher SDH activity than OHT alone and OHT mice injected with AAV2:eGFP (Figure 8E; $p < 0.001$, $p < 0.05$ respectively). OHT mice injected with AAV2:MCT2 also have significantly higher COX activity than OHT mice (Figure 8F, $p < 0.0001$).

3.9   MCT2 Overexpression Protected Inner Retinal Function after OHT

Microglia density does not differ between OHT mice injected with AAV2:eGFP or AAV2:MCT2 (Figure 9A). However, there is a significant effect of virus injection lowering Iba1 fluorescence intensity across the OHT groups (Figure 9B, $p < 0.0001$). OHT mice injected with AAV2:MCT2 had significantly higher pattern electroretinogram P1 peak amplitude than OHT mice (Figure 9C, $p < 0.05$). N2 amplitude shows no difference across the control and experimental groups (Figure 9D). Representative PERG traces for each analyzed group are shown in Figure 9E.

4.   Discussion

Reduction of MCT2 in the retina through cre-mediated elimination of flox'd MCT2 alleles resulted in compromised ATP production and visual evoked potential. These findings corroborate our observations of the significant, negative impact of MCT2 decrease in mouse models of glaucoma (Harun-or-Rashid et al., 2018), and motivated our strategy to increase metabolic substrate availability in the visual system through overexpression of MCT2. Using AAV2 to increase MCT2 expression in the retina and ON of D2 mice and those with OHT resulted in rescue of RGC soma and axon number, restoration of energy homeostasis, and increased mitochondrial activity.

The kinetics of MCT2 indicates the transporter has a high affinity for monocarboxylates (Bröer et al., 1999), a quality associated with a cell type that imports, rather than exports, monocarboxylates. RGCs and Müller glia are likely importers of monocarboxylates, the latter because their pyruvate kinase deficiency necessitates carbon sources others than glucose to fuel their oxidative phosphorylation (Lindsay et al., 2014). Gerhart et al, concluded that MCT2 was only associated with glial cells despite showing immunolabeling that included RGCs (Gerhart et al., 1999). We have demonstrated MCT2 expression on RGCs and their axons (Harun-or-Rashid et al., 2018) and adopted an AAV2-mediated infection strategy that was designed to overexpress MCT2 in RGCs. We observed no AAV2-associated GFP reporter expression in cells other than neurons in the retina.

Since MCT2 transports ketone bodies in addition to lactate and pyruvate, we asked ourselves whether greater availability of ketone bodies in the bloodstream would be necessary for the potential improvement in energy homeostasis in the AAV2:MCT2 injected mice. Significant protection of RGC somata was observed in D2 mice on the ketogenic diet injected with AAV2:MCT2; however, we observed a negative impact on axon number of the ketogenic diet on the D2 mice with AAV2:MCT2 infection. There were a few optic nerves with normal numbers of RGC axons, but the majority showed no difference in axon number from untreated D2 mice. This was surprising as it suggests the viral overexpression counteracted

the D2 axon protection observed with the ketogenic diet in past publications (Harun-or-Rashid et al., 2018). One potential explanation was the significant increase in Iba1+ cell number and fluorescence intensity, an indication of microglial activation, that was observed in the mice injected with AAV2:MCT2. A prominent effect of the ketogenic diet is its inhibition of NF-κB signaling and the NLRP3 inflammasome through HCAR1, a ketone body receptor expressed on microglia, among other cells (Harun-or-Rashid and Inman, 2018). It is likely that the virus-mediated inflammatory response overcame the anti-inflammatory effect of the ketogenic diet, resulting in greater axon loss. Mice on the ketogenic diet have a significant proportion of microglia with an anti-inflammatory phenotype (Harun-or-Rashid and Inman, 2018), while untreated D2 mice have primarily microglia with a pro-inflammatory phenotype (Wilson et al., 2015). The virus may have promoted a transition of the anti-inflammatory microglia to pro-inflammatory phenotypes by triggering NF-κB signaling in the ketogenic diet group. Having the ketogenic diet group undergo a significant microglial phenotypic shift while the untreated D2 microglia underwent no shift could explain the discrepancy. Microglial phenotype relies on the sequence and duration of initiating stimuli (Perry et al., 2010), suggesting that the ketogenic diet context ensured subsequent response to virus injection would diverge from mice on standard lab chow. One important difference between our past ketogenic study and this one was the age of the D2 mice; they were 11 months of age at analysis in the prior study, but 12 months of age in this study, so likely to have a more progressed glaucoma pathology. Given the magnitude of the RGC protection in older mice here, the MCT2 overexpression may be of greater benefit than the ketogenic diet to RGC survival and function. Ultimately, we were able to determine that the virus-mediated MCT2 expression did not require the diet to be effective.

It was our expectation that we would observe a decline in hexokinase activity with AAV2:MCT2 injection because we hypothesized that increased MCT2 would lead to greater monocarboxylate import, increased mitochondrial function and lowered glycolysis. The OHT mice injected with AAV2:MCT2 had significantly lower hexokinase activity than OHT alone. Since control virus injected OHT eyes had similar hexokinase activity as the OHT alone, it was evident that the addition of MCT2 was associated with the decline in hexokinase activity. The AAV2:MCT2 OHT ON achieved energy homeostasis (low pAMPK/AMPK ratio), and the SDH and COX activities were significantly greater than OHT alone, indicating that mitochondrial function was indeed higher in the AAV2:MCT2 OHT ON. However, hexokinase activity was significantly upregulated in the AAV2:MCT2 D2 ON compared to untreated D2. For the D2, it may be the case that the improvement in energy homeostasis (evident with the decline in pAMPK/AMPK ratio) enabled improved function for all modes of ATP generation, glycolysis and oxidative phosphorylation. Another possibility is that the D2 ON, relying heavily on glycolysis as we have demonstrated in prior studies (Jassim et al., 2019), would not have experienced an increase in monocarboxylate import through MCT2 sufficient enough to displace the energy that could be obtained through glycolysis. Alternatively, the upregulation of MCT2 in RGC axons might have created a lactate sink, allowing the astrocytes and oligodendrocytes to engage in higher rates of glycolysis. The more advanced glial pathology of the 12-month-old D2 mice compared to the mice with OHT would contribute most of the hexokinase activity measured in whole

ON. Important to note is that the observed changes in hexokinase activity are relative; the hexokinase activity in the D2 ON with AAV2:MCT2, despite being significantly higher than untreated D2, was still lower than the control ON in the OHT experiment.

PGC-1α was significantly upregulated in ON after AAV2:MCT2 injection in retina for the D2 model of glaucoma. PGC1α can contribute in significant ways to cellular protection in glaucoma (Guo et al., 2014; Harun-or-Rashid et al., 2018) by suppressing reactive oxygen species (ROS) generation through expression of ROS scavenging enzymes such as SOD2 (St-Pierre et al., 2006). PGC1α also coordinates mitochondrial biogenesis by coactivating TFAM (mitochondrial transcription factor A), a direct regulator of mtDNA transcription (Wu et al., 1999). Consistent with no significant change in the PGC1α expression in the AAV2:MCT2+OHT group, we observed no differences in mitochondrial size or density in the retina. Though we did not evaluate mitochondria in the D2 mice, we did observe significant increases in succinate dehydrogenase (SDH) activity in the D2 with AAV2:MCT2 injection. SDH is part of the TCA cycle and the mitochondrial electron transport chain; its activity is a proxy for mitochondrial function. In the OHT groups, AAV2:MCT2 infection increased the SDH activity above OHT alone, but it did not reach the level of control ON. The high SDH and cytochrome c oxidase activities in ONs from AAV2:MCT2 injected mice indicate MCT2 overexpression allowed for import of various energy substrates that could be utilized by mitochondria for TCA cycle and electron transport chain function.

One drawback of viral vectors is the possibility of engendering an inflammatory response. Microglial density increased in D2 retina with AAV2:MCT2 infection, regardless of diet. There was no change in microglial density in OHT retina with or without AAV2:MCT2 infection. This difference between D2 and OHT microglia density was not unexpected for the D2, given the significant inflammatory response observed in the D2 retina (Bosco et al., 2011, 2008). Toll-like receptors mediate the initial immune response to AAV (Zhu et al., 2009), including NF-κB activation with downstream cytokine production (Rogers et al., 2011). Cytokines such as TNFα, IL-6, IFNα/β, and MCP-2 released from AAV capsid-ingesting antigen presenting cells (Rogers et al., 2011) have been observed in glaucomatous retina and ON (Chidlow et al., 2012; Tezel et al., 2001; Wilson et al., 2015). Despite the limited data on antigen presenting cells in retina, the potential for additional cytokine release raises the possibility that AAV injection would exacerbate immune response there. However, the absence of microglial density change and the significant decline in microglial Iba1 intensity with AAV2:MCT2 after OHT suggest the virus was not as directly immunogenic as it appeared to be with the D2 mouse. As mentioned above, the virus infection was likely to have reversed the anti-inflammatory effect of the ketogenic diet.

MCT inhibition using α-cyano-4-hydroxycinnamate resulted in a reduction of the flash ERG b-wave and associated oscillatory potentials (B. V. Bui et al., 2004), suggesting that glutamatergic neurotransmission from photoreceptors to bipolar cells was negatively impacted by inhibition of monocarboxylate transport. The implication is that glutamate would have been shunted from the glutamate-glutamine cycle to contributing to the TCA cycle. It is also the case that the b-wave receives contribution from Müller glia (Byrne et al., 2013; Wen and Oakley, 1990), and inhibiting Müller glial uptake of lactate from

photoreceptors (Lindsay et al., 2014) could also explain the reduction. In this study, pattern electroretinogram showed a P1 amplitude that was significantly higher in the AAV2:MCT2 mouse with OHT compared to OHT alone. There was a trend toward greater N2 amplitude with AAV2:MCT2 infection, but it was not statistically different from control or OHT alone. The significance of the P1 amplitude is unknown since the source of the individual components of the PERG waveform has not been established (Porciatti, 2007).

5. Conclusion

Facilitating the transport of monocarboxylates in the retina during ocular hypertension, either through short-term (4 weeks) or long-term (6 months) IOP increase, maintained RGC number, improved energy homeostasis, and increased mitochondrial function in the retina and ON. These findings indicate metabolic intervention to support visual function is a viable approach for the treatment of glaucoma.

Acknowledgements:

References

Baltan S, Inman D, Danilov C, Morrison R, Calkins D, Horner P, 2010 Metabolic vulnerability disposes retinal ganglion cell axons to dysfunction in a model of glaucomatous degeneration. J. Neurosci 30, 5644–5652. 10.1523/JNEUROSCI.5956-09.2010 [PubMed: 20410117]

Bosco A, Inman DM, Steele MR, Wu G, Soto I, Marsh-Armstrong N, Hubbard WC, Calkins DJ, Horner PJ, Vetter ML, 2008 Reduced retina microglial activation and improved optic nerve integrity with minocycline treatment in the DBA/2J mouse model of glaucoma. Invest Ophthalmol Vis Sci 49, 1437–1446. https://doi.org/18385061 [PubMed: 18385061]

Bosco A, Steele MR, Vetter ML, 2011 Early microglia activation in a mouse model of chronic glaucoma. J. Comp. Neurol 519, 599–620. 10.1002/cne.22516.Early [PubMed: 21246546]

Bough KJ, Wetherington J, Hassel B, Pare JF, Gawryluk JW, Greene JG, Shaw R, Smith Y, Geiger JD, Dingledine RJ, 2006 Mitochondrial biogenesis in the anticonvulsant mechanism of the ketogenic diet. Ann. Neurol 60, 223–35. 10.1002/ana.20899 [PubMed: 16807920]

Bouzier-Sore AK, Voisin P, Bouchaud V, Bezancon E, Franconi JM, Pellerin L, 2006 Competition between glucose and lactate as oxidative energy substrates in both neurons and astrocytes: A comparative NMR study. Eur. J. Neurosci 24, 1687–1694. 10.1111/j.1460-9568.2006.05056.x [PubMed: 17004932]

Bröer S, Bröer A, Schneider HP, Stegen C, Halestrap AP, Deitmer JW, 1999 Characterization of the high-affinity monocarboxylate transporter MCT2 in Xenopus laevis oocytes. Biochem. J 341, 529–535. 10.1042/0264-6021:3410529 [PubMed: 10417314]

Buckingham BP, Inman DM, Lambert WS, Oglesby E, Calkins DJ, Steele MR, Vetter ML, Marsh-Armstrong N, Horner PJ, 2008 Progressive ganglion cell degeneration precedes neuronal loss in a mouse model of glaucoma. J Neurosci 28, 2735–2744. https://doi.org/18337403 [PubMed: 18337403]

Bui BV, Kalloniatis M, Vingrys AJ, 2004 Retinal Function Loss after Monocarboxylate Transport Inhibition. Investig. Ophthalmol. Vis. Sci 45, 584–593. 10.1167/iovs.03-0695 [PubMed: 14744902]

Bui BV, Vingrys AJ, Wellard JW, Kalloniatis M, 2004 Monocarboxylate transport inhibition alters retinal function and cellular amino acid levels. Eur. J. Neurosci 20, 1525–1537. 10.1111/j.1460-9568.2004.03601.x [PubMed: 15355319]

Byrne LC, Khalid F, Lee T, Zin EA, Greenberg KP, Visel M, Schaffer DV, Flannery JG, 2013 AAV-Mediated, Optogenetic Ablation of Müller Glia Leads to Structural and Functional Changes in the Mouse Retina. PLoS One 8, 1–13. 10.1371/journal.pone.0076075

Chenal J, Pierre K, Pellerin L, 2007 Insulin and IGF-1 enhance the expression of the neuronal monocarboxylate transporter MCT2 by translational activation via stimulation of the phosphoinositide 3-kinase-Akt-mammalian target of rapamycin pathway. Eur. J. Neurosci 27, 53–65. 10.1111/j.1460-9568.2007.05981.x [PubMed: 18093179]

Chidlow G, Wood JPM, Ebneter A, Casson RJ, 2012 Interleukin-6 is an efficacious marker of axonal transport disruption during experimental glaucoma and stimulates neuritogenesis in cultured retinal ganglion cells. Neurobiol. Dis 48, 568–81. 10.1016/j.nbd.2012.07.026 [PubMed: 22884876]

Crish SD, Sappington RM, Inman DM, Horner PJ, Calkins DJ, 2010 Distal axonopathy with structural persistence in glaucomatous neurodegeneration. Proc. Natl. Acad. Sci. U. S. A 107, 5196–201. 10.1073/pnas.0913141107 [PubMed: 20194762]

Dutta DJ, Ho D, Lee PR, Pajevic S, Bukalo O, Huffman WC, Wake H, Basser PJ, SheikhBahaei S, Lazarevic V, Smith JC, Fields RD, 2018 Regulation of myelin structure and conduction velocity by perinodal astrocytes. Proc Natl Acad Sci U S A 115, 11832–11837. 10.1073/pnas.1811013115 [PubMed: 30373833]

Gerhart DZ, Leino RL, Drewes LR, 1999 Distribution of monocarboxylate transporters MCT1 and MCT2 in rat retina. Neuroscience 92, 367–375. 10.1016/S0306-4522(98)00699-X [PubMed: 10392858]

Guo X, Dason ES, Zanon-Moreno V, Jiang Q, Nahirny A, Chan D, Flanagan JG, Sivak JM, 2014 PGC-1α Signaling Coordinates Susceptibility to Metabolic and Oxidative Injury in the Inner Retina. Am. J. Pathol 184, 1017–1029. 10.1016/j.ajpath.2013.12.012 [PubMed: 24508229]

Halestrap AP, 2013a Monocarboxylic acid transport. Compr. Physiol 3, 1611–43. 10.1002/cphy.c130008 [PubMed: 24265240]

Halestrap AP, 2013b The SLC16 gene family - Structure, role and regulation in health and disease. Mol. Aspects Med 34, 337–349. 10.1016/j.mam.2012.05.003 [PubMed: 23506875]

Halestrap AP, Meredith D, 2004 The SLC16 gene family - From monocarboxylate transporters (MCTs) to aromatic amino acid transporters and beyond. Pflugers Arch. Eur. J. Physiol 447, 619–628. 10.1007/s00424-003-1067-2 [PubMed: 12739169]

Harun-or-Rashid M, Inman DM, 2018 Reduced AMPK activation and increased HCAR activation drives anti-inflammatory response and neuroprotection in glaucoma. J. Neuroinflammation 15, 313–327. [PubMed: 30424795]

Harun-or-Rashid M, Pappenhagen N, Palmer PG, Smith MA, Gevorgyan V, Wilson GN, Crish SD, Inman DM, 2018 Structural and Functional Rescue of Chronic Metabolically Stressed Optic Nerves through Respiration. J. Neurosci 38, 5122–5139. 10.1523/JNEUROSCI.3652-17.2018 [PubMed: 29760184]

Howell GR, Libby RT, John SW, 2008 Mouse genetic models: an ideal system for understanding glaucomatous neurodegeneration and neuroprotection. Prog Brain Res 173, 303–321. [PubMed: 18929118]

Howell GR, Libby RT, Marchant JK, Wilson L. a, Cosma IM, Smith RS, Anderson MG, John SWM, 2007 Absence of glaucoma in DBA/2J mice homozygous for wild-type versions of Gpnmb and Tyrp1. BMC Genet. 8, 45 10.1186/1471-2156-8-45 [PubMed: 17608931]

Imai Y, Kohsaka S, 2002 Intracellular signaling in M-CSF-induced microglia activation: Role of Iba1. Glia 40, 164–174. 10.1002/glia.10149 [PubMed: 12379904]

Ito D, Imai Y, Ohsawa K, Nakajima K, Fukuuchi Y, Kohsaka S, 1998 Microglia-specific localisation of a novel calcium binding protein, Iba1. Brain Res Mol Brain Res 57, 1–9. [PubMed: 9630473]

Jassim AH, Coughlin L, Harun-or-rashid M, Kang PT, Chen Y, Inman DM, 2019 Higher Reliance on Glycolysis Limits Glycolytic Responsiveness in Degenerating Glaucomatous Optic Nerve. Mol. Neurobiol 56, 7097–7112. [PubMed: 30980229]

Lee Y, Morrison BM, Li Y, Lengacher S, Farah MH, Hoffman PN, Liu Y, Tsingalia A, Jin L, Zhang P, Pellerin L, Magistretti PJ, Rothstein JD, 2012 Oligodendroglia metabolically support axons and

contribute to neurodegeneration. Nature 487, 443–448. 10.1038/nature11314.Oligodendroglia [PubMed: 22801498]

Lindsay KJ, Du J, Sloat SR, Contreras L, Linton JD, Turner SJ, Sadilek M, Satrustegui J, Hurley JB, Satrústegui J, Hurley JB, 2014 Pyruvate kinase and aspartate-glutamate carrier distributions reveal key metabolic links between neurons and glia in retina. Proc. Natl. Acad. Sci 111, 15579–15584. 10.1073/pnas.1412441111 [PubMed: 25313047]

Mächler P, Wyss MT, Elsayed M, Stobart J, Gutierrez R, Von Faber-Castell A, Kaelin V, Zuend M, San Martín A, Romero-Gómez I, Baeza-Lehnert F, Lengacher S, Schneider BL, Aebischer P, Magistretti PJ, Barros LF, Weber B, 2016 In Vivo Evidence for a Lactate Gradient from Astrocytes to Neurons. Cell Metab. 23, 94–102. 10.1016/j.cmet.2015.10.010 [PubMed: 26698914]

Manoharan C, Wilson MC, Sessions RB, Halestrap AP, 2006 The role of charged residues in the transmembrane helices of monocarboxylate transporter 1 and its ancillary protein basigin in determining plasma membrane expression and catalytic activity. Mol. Membr. Biol 23, 486–498. 10.1080/09687860600841967 [PubMed: 17127621]

Melena J, Safa R, Graham M, Casson RJ, Osborne NN, 2003 The monocarboxylate transport inhibitor, α-cyano-4-hydroxycinnamate, has no effect on retinal ischemia. Brain Res. 989, 128–134. 10.1016/S0006-8993(03)03375-4 [PubMed: 14519520]

Ovens MJ, Manoharan C, Wilson MC, Murray CM, Halestrap AP, 2010 The inhibition of monocarboxylate transporter 2 (MCT2) by AR-C155858 is modulated by the associated ancillary protein. Biochem. J 431, 217–225. 10.1042/BJ20100890 [PubMed: 20695846]

Perry VH, Nicoll JAR, Holmes C, 2010 Microglia in neurodegenerative disease. Nat. Rev. Neurol 6, 193–201. 10.1038/nrneurol.2010.17 [PubMed: 20234358]

Pierre K, Magistretti PJ, Pellerin L, 2002 MCT2 is a major neuronal monocarboxylate transporter in the adult mouse brain. J. Cereb. Blood Flow Metab 22, 586–95. 10.1097/00004647-200205000-00010 [PubMed: 11973431]

Porciatti V, 2007 The mouse pattern electroretinogram. Doc Ophthalmol 115, 145–153. [PubMed: 17522779]

Rafiki A, Boulland JL, Halestrap AP, Ottersen OP, Bergersen L, 2003 Highly differential expression of the monocarboxylate transporters MCT2 and MCT4 in the developing rat brain. Neuroscience 122, 677–688. 10.1016/j.neuroscience.2003.08.040 [PubMed: 14622911]

Rogers GL, Martino AT, Aslanidi GV, Jayandharan GR, Srivastava A, Herzog RW, 2011 Innate immune responses to AAV vectors. Front. Microbiol 2, 1–10. 10.3389/fmicb.2011.00194 [PubMed: 21716958]

Saab AS, Tzvetavona ID, Trevisiol A, Baltan S, Dibaj P, Kusch K, Möbius W, Goetze B, Jahn HM, Huang W, Steffens H, Schomburg ED, Pérez-Samartín A, Pérez-Cerdá F, Bakhtiari D, Matute C, Löwel S, Griesinger C, Hirrlinger J, Kirchhoff F, Nave K-A, 2016 Oligodendroglial NMDA Receptors Regulate Glucose Import and Axonal Energy Metabolism. Neuron 91, 119–132. 10.1016/j.neuron.2016.05.016 [PubMed: 27292539]

Serwanski DR, Jukkola P, Nishiyama A, 2017 Heterogeneity of astrocyte and NG2 cell insertion at the node of ranvier. J. Comp. Neurol 525, 535–552. 10.1002/cne.24083 [PubMed: 27448245]

Siesjö BK, 1978 Brain energy metabolism and catecholaminergic activity in hypoxia, hypercapnia and ischemia. J. Neural Transm. Suppl 17–22. [PubMed: 290738]

Simpson IA, Carruthers A, Vannucci SJ, 2007 Supply and demand in cerebral energy metabolism: the role of nutrient transporters. J Cereb Blood Flow Metab. 27, 1766–1791. 10.1038/sj.jcbfm.9600521 [PubMed: 17579656]

St-Pierre J, Drori S, Uldry M, Silvaggi JM, Rhee J, Jaeger S, Handschin C, Zheng K, Lin J, Yang W, Simon DK, Bachoo R, Spiegelman BM, 2006 Suppression of Reactive Oxygen Species and Neurodegeneration by the PGC-1 Transcriptional Coactivators. Cell 127, 397–408. 10.1016/j.cell.2006.09.024 [PubMed: 17055439]

Takimoto M, Hamada T, 2014 Acute exercise increases brain region-specific expression of MCT1, MCT2, MCT4, GLUT1, and COX IV proteins. J. Appl. Physiol 116, 1238–50. 10.1152/japplphysiol.01288.2013 [PubMed: 24610532]

Tanner LB, Goglia AG, Wei MH, Sehgal T, Parsons LR, Park JO, White E, Toettcher JE, Rabinowitz JD, 2018 Four Key Steps Control Glycolytic Flux in Mammalian Cells. Cell Syst. 7, 49–62.e8. 10.1016/j.cels.2018.06.003 [PubMed: 29960885]

Tezel G, Li LY, Patil RV, Wax MB, 2001 TNF-alpha and TNF-alpha receptor-1 in the retina of normal and glaucomatous eyes. Invest Ophthalmol Vis Sci 42, 1787–1794. [PubMed: 11431443]

Wen R, Oakley B, 1990 K+-evoked Müller cell depolarization generates b-wave of electroretinogram in toad retina. Proc. Natl. Acad. Sci. U. S. A 87, 2117–2121. 10.1073/pnas.87.6.2117 [PubMed: 2107544]

Williams PA, Harder JM, Foxworth NE, Cochran KE, Philip VM, Porciatti V, Smithies O, John SWM, 2017 Vitamin B3 modulates mitochondrial vulnerability and prevents glaucoma in aged mice. Science 760, 756–760. 10.1120/science.aal0092

Wilson G, Inman D, Denger-Crish C, Smith M, Crish S, 2015 Early pro-inflammatory cytokine elevations in the DBA/2J mouse model of glaucoma. J. Neuroinflammation 12 10.1186/s12974-015-0399-0

Wilson MC, Kraus M, Marzban H, Sarna JR, Wang Y, Hawkes R, Halestrap AP, Beesley PW, 2013 The neuroplastin adhesion molecules are accessory proteins that chaperone the monocarboxylate transporter MCT2 to the neuronal cell surface. PLoS One 8 10.1371/journal.pone.0078654

Wilson MC, Meredith D, Fox JEM, Manoharan C, Davies AJ, Halestrap AP, 2005 Basigin (CD147) Is the Target for Organomercurial Inhibition of Monocarboxylate Transporter Isoforms 1 and 4 280, 27213–27221. 10.1074/jbc.M411950200

Wu Z, Puigserver P, Andersson U, Zhang C, Adelmant G, Mootha V, Troy A, Cinti S, Lowell B, Scarpulla RC, Spiegelman BM, 1999 Mechanisms controlling mitochondrial biogenesis and respiration through the thermogenic coactivator PGC-1. Cell 98, 115–124. 10.1016/S0092-8674(00)80611-X [PubMed: 10412986]

Yang C, Jiang L, Zhang H, Shimoda LA, Deberardinis RJ, Semenza GL, 2014 Analysis of hypoxia-induced metabolic reprogramming, Methods in Enzymology. 10.1016/B978-0-12-416618-9.00022-4

Zhu J, Huang X, Yang Y, 2009 The TLR9-MyD88 pathway is critical for adaptive immune responses to adenoassociated virus gene therapy vectors in mice. J. Clin. Invest 119, 2388–2398. 10.1172/JCI37607 [PubMed: 19587448]

Highlights:

- Loss of MCT2 in retina compromises visual function and ATP production in optic nerve

- MCT2 overexpression preserves RGC soma and axon number in two glaucoma models

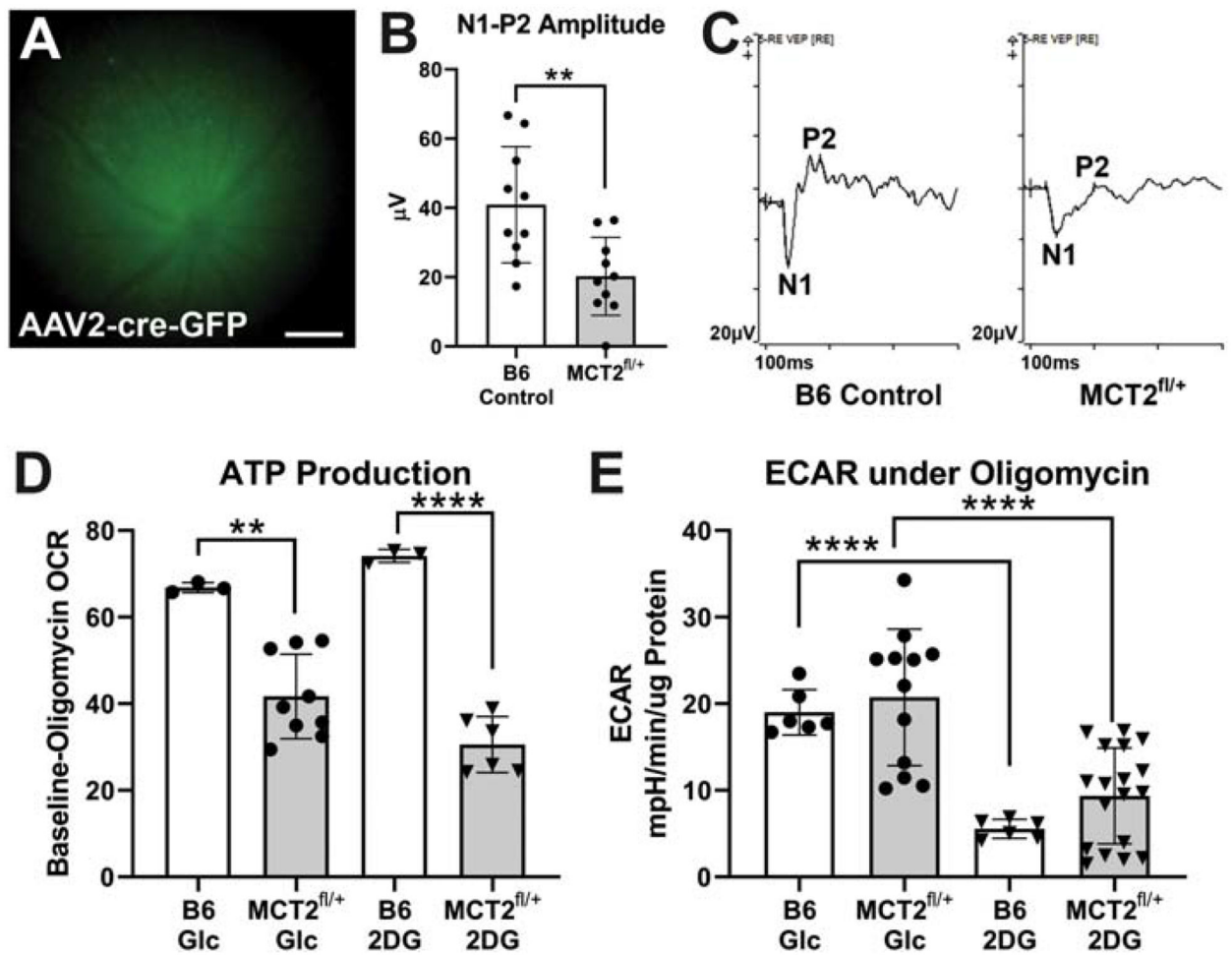- MCT2 overexpression improves energy homeostasis in optic nerve

Figure 1:

Visual evoked potential (VEP) and optic nerve (ON) metabolism in MCT2$^{fl/+}$ mice. **A**. MCT2$^{fl/+}$ mouse eyes injected with AAV2-cre-GFP were imaged to show expression of GFP in the ganglion cell layer two weeks after infection. Successful cre recombination removes one MCT2 allele from infected cells. Scale bar= 200μm. **B**. VEP response amplitude was significantly reduced in MCT2$^{fl/+}$ mice (n=10; p<0.01) compared to age-matched C56Bl/6 (B6) control mice (n=10). **C**. Representative VEP traces in B6 control (left) and MCT2$^{fl/+}$ (right) mice. Response amplitude is the μV difference between the N1 trough and the P2 peak. **D**. The difference in baseline versus oligomycin-treatment oxygen consumption rate (OCR) calculated from the ONs of B6 control (n=3) or MCT2$^{fl/+}$ mice (n=9) were significantly different for the ONs incubated in glucose (Glc; p<0.1) and 2-deoxyglucose (2-DG; p<0.001). **E**. Extracellular acidification rate (ECAR) was similar for B6 control (n=6) and MCT2$^{fl/+}$ (n=18) *within* the Glc or the 2-DG groups, but the 2-DG groups for each were significantly reduced compared to Glc (p<0.0001). Error bars are SD.
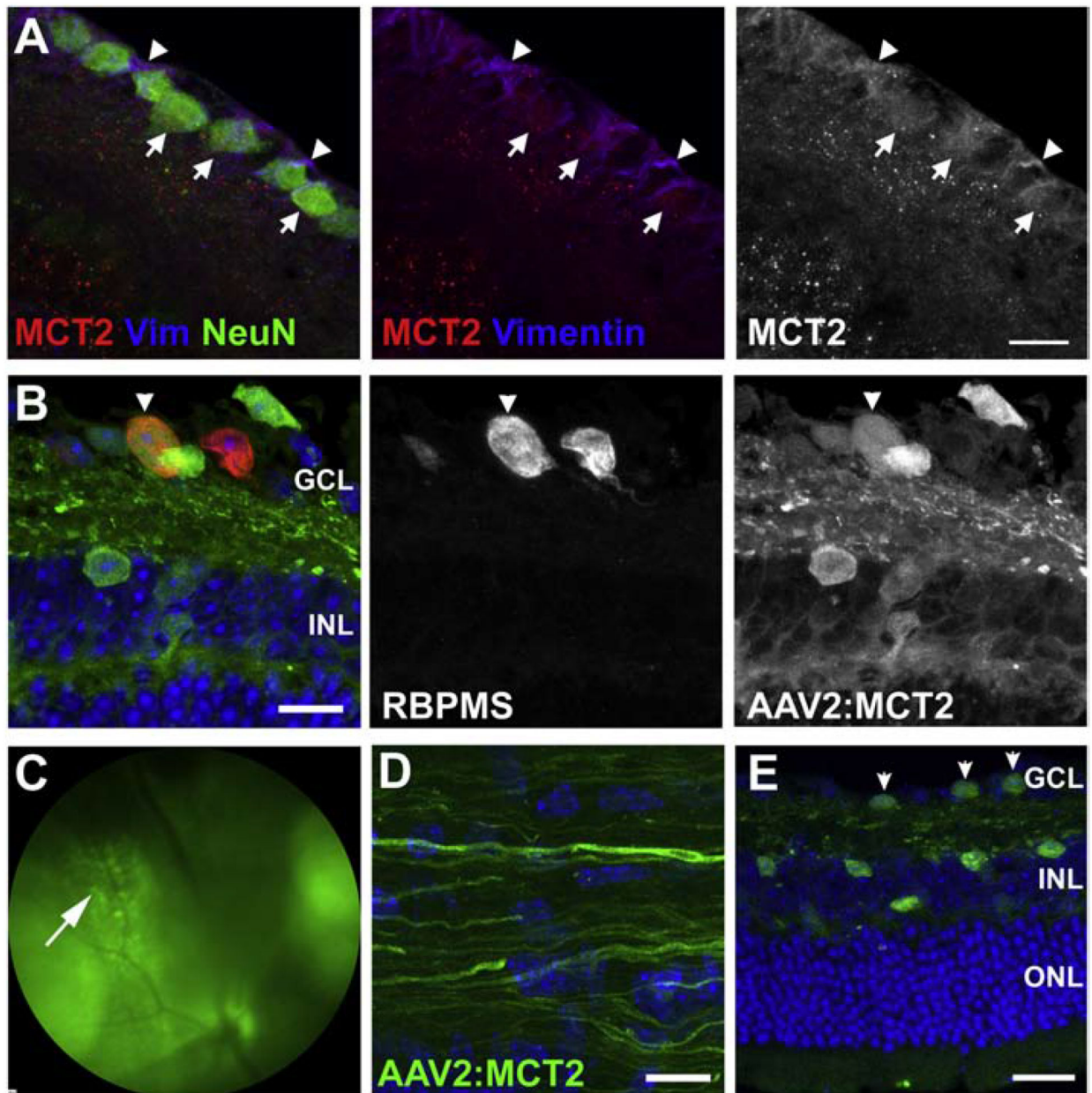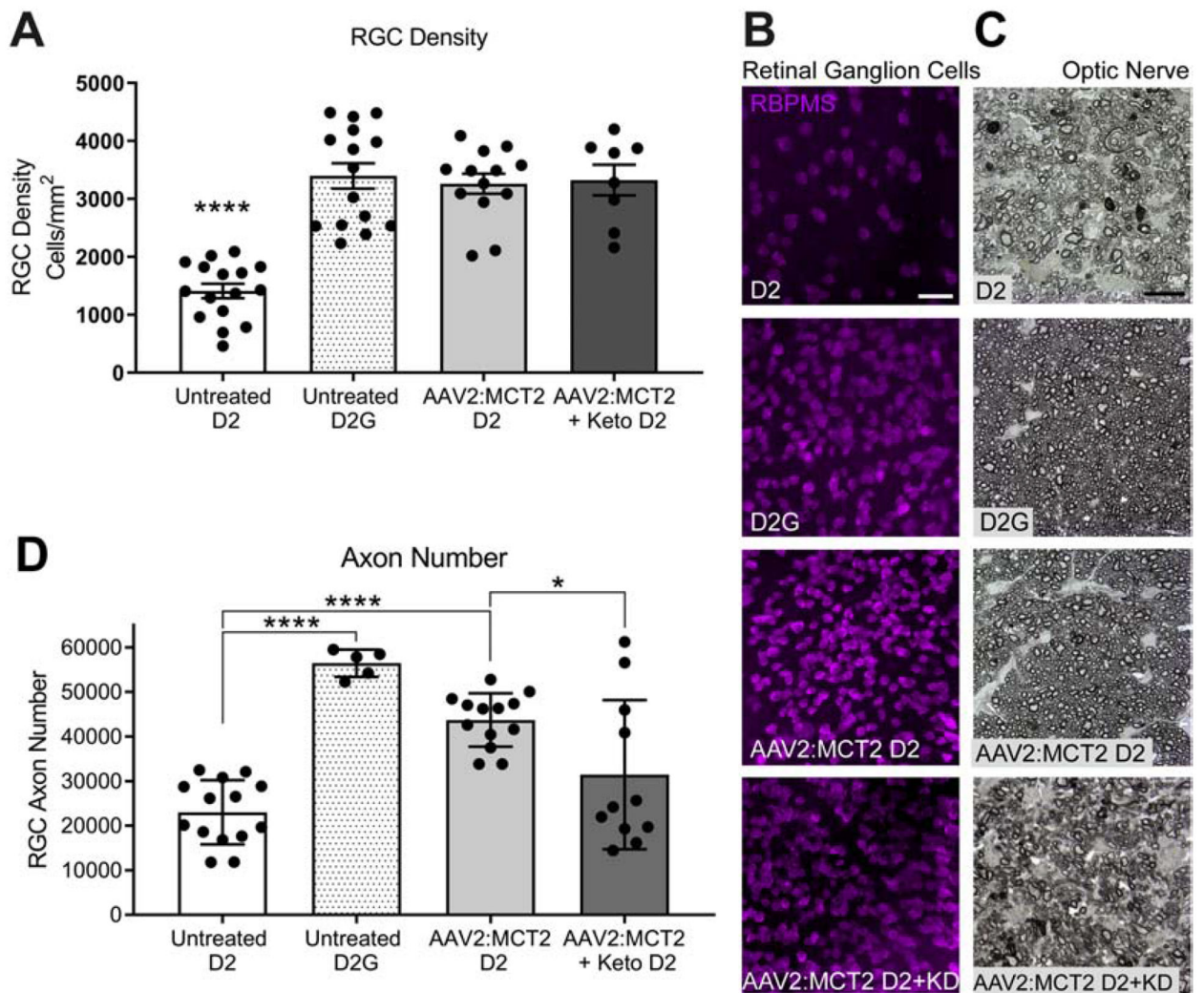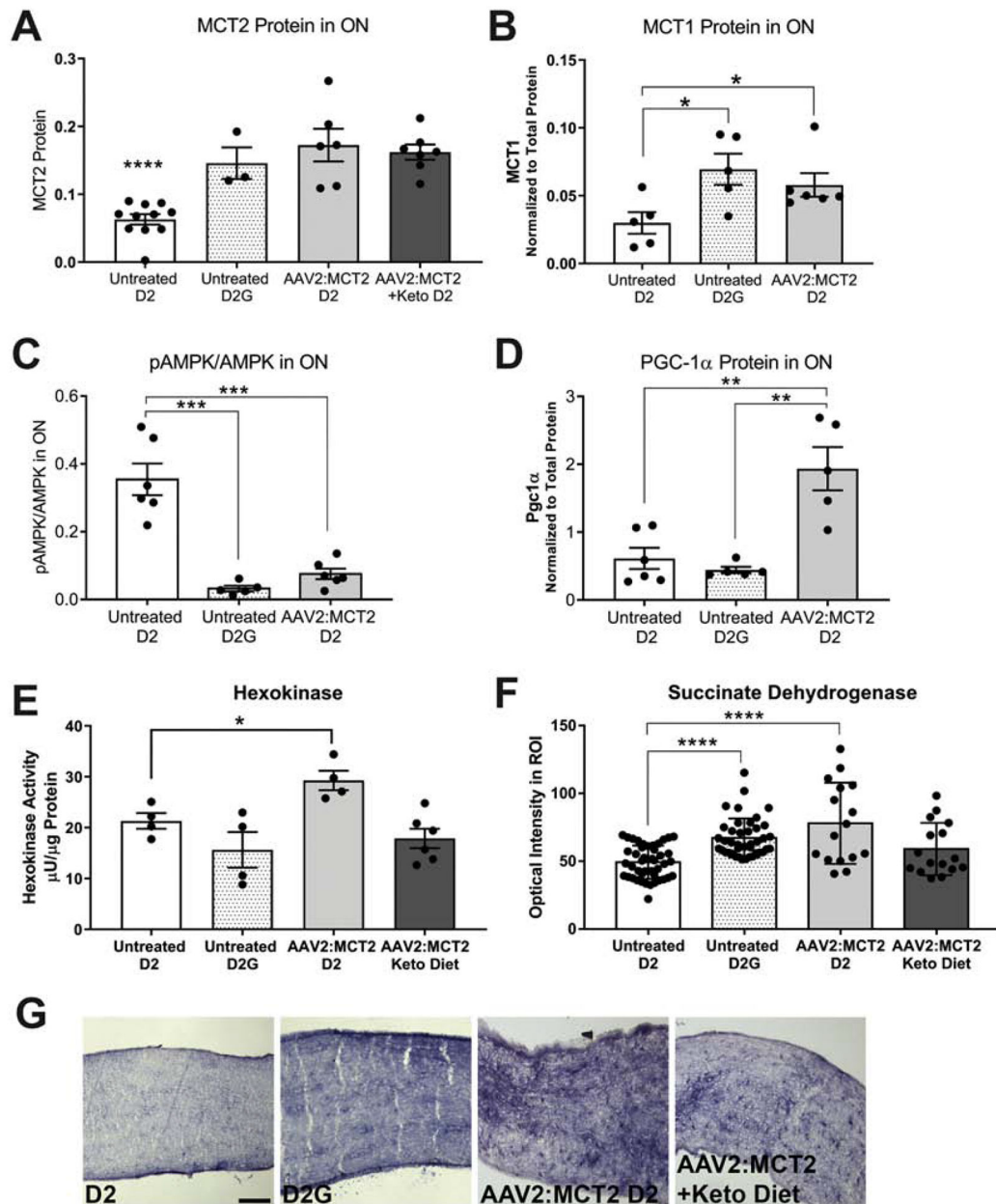
Figure 2:

MCT2 protein distribution and AAV2:MCT2 virus infection. **A**. Immunofluorescence of control retina to show MCT2 localization on retinal ganglion cells. The left panel is a merged image of MCT2 (red) with Vimentin (Müller glia, blue) and NeuN (RGCs, green). In the middle panel, NeuN has been removed in order to discern the red puncta along both RGC somas and Müller glia endfeet. The right panel shows MCT2 alone. Scale bar is 15μM. **B**. A cross-section from a 12 month-old D2 retina injected with AAV2:MCT2 two months prior. Arrowheads point to an infected RGC in the GCL that is RBPMS-positive and positive for the eGFP from the AAV2:MCT2 virus. INL=inner nuclear layer; OPL=outer plexiform layer. Scale bar=15μm. **C**. Fundus photograph of a 10.5 month-old DBA/2J (D2) eye injected with AAV2:MCT2, two weeks after injection (left). The arrow points to GFP-

positive cells in the ganglion cell layer (GCL). **D**. Section of a 12 month-old D2 optic nerve from an eye injected with AAV2:MCT2. The eGFP-positive axons confirm the infection of RGCs with the virus and the widespread transport of the eGFP. Scale bar=20μm. **E**. Sagittal section of a 12 month-old D2 retina injected with AAV2:MCT2 two months prior. Arrows point to infected cells in the GCL that are eGFP-positive from the AAV2:MCT2 virus. Infected cells are observed in the GCL and INL. Scale bar=50μm. GCL=ganglion cell layer; INL=inner nuclear layer; OPL=outer plexiform layer.

Figure 3:

Retinal ganglion cell soma and axon quantification and integrity. **A**. Retinal ganglion cell density (cells/mm^2) in 12 month-old D2 retina (n=16), age-matched control strain DBA/2-*Gpnmb*[+] (D2G) retina (n=15), 12 month-old D2 retina injected with AAV2:MCT2 (n=13), and 12 month-old D2 retina injected with AAV2:MCT2 and placed on a ketogenic diet for 8 weeks (n=8). D2G and both virus injected groups have significantly greater RGC density than 12 month-old D2 (p<0.0001). **B**. Wholemount retina immunolabeled for RBPMS, an RGC-specific marker, from untreated D2 and D2G retina, and D2 mouse retina injected with AAV2:MCT2, with or without the ketogenic diet (KD). Images were taken 1mm from the optic nerve head. Scale bar=25μm. **C**. Cross-sections of ρ-phenylenediamine labeled optic nerve from untreated D2 and D2G, then D2 mice injected with AAV2:MCT2, with or without the ketogenic diet (KD). Scale bar=10μm. **D**. Optic nerve (ON) axon counts from D2 (n=14), D2G (n=5), and D2 injected with AAV2:MCT2, with (n=11) or without (n=13) the ketogenic diet. D2 axon number is significantly lower than D2G and AAV2:MCT2 D2 (p<0.0001). AAV2:MCT2 D2 mice on the ketogenic diet had significantly lower ON axon number than the AAV2:MCT2 D2 mice on normal rodent chow (p<0.05). Error bars are SD.

Figure 4:

Protein and metabolic changes in optic nerve (ON) from D2 mice injected with AAV2:MCT2. **A**. MCT2 protein in ON from D2 (n=11), D2G mice (n=3), and D2 mice injected with AAV2:MCT2, with (n=7) or without (n=6) the ketogenic diet. Untreated D2 MCT2 protein is significantly lower (p<0.0001) than each of the other experimental groups depicted. **B**. MCT1 expression is higher in both untreated D2G (n=5) and AAV2:MCT2 injected D2 (n=6) than in untreated D2 (n=5) optic nerve (p<0.05). **C**. pAMPK/AMPK ratio is significantly higher in untreated D2 (n=6) than D2G (n=5) and AAV2:MCT2 injected D2 (n=6) mice (p<0.001). **D**. PGC-1α is upregulated in D2 mice injected with AAV2:MCT2 (n=5) compared to both untreated D2 (n=5) and D2G mice (n=6) (p<0.01). **E**. Hexokinase activity is significantly increased in AAV2:MCT2 injected D2 mice (n=4) compared to

untreated D2 (n=4). Untreated D2G (n=4) and D2 mice injected with AAV2:MCT2 on the ketogenic diet (n=6) are not different from untreated D2 (p<0.05). **F**. Succinate dehydrogenase activity is significantly decreased in untreated D2 (n=32 sections from 8 ON) mouse ON compared to both untreated D2G (n=36 sections from 8 ON) and AAV2:MCT2 treated D2 mice on standard chow (control diet; n=16 sections from 5 ON), p<0.0001. For the AAV2:MCT2 injected D2 mouse on the ketogenic diet, 16 sections from 5 ON were analyzed. **G**. Succinate dehydrogenase histochemistry of example ONs from groups as shown in panel F. Scale bar=250μm. Error bars are SD.
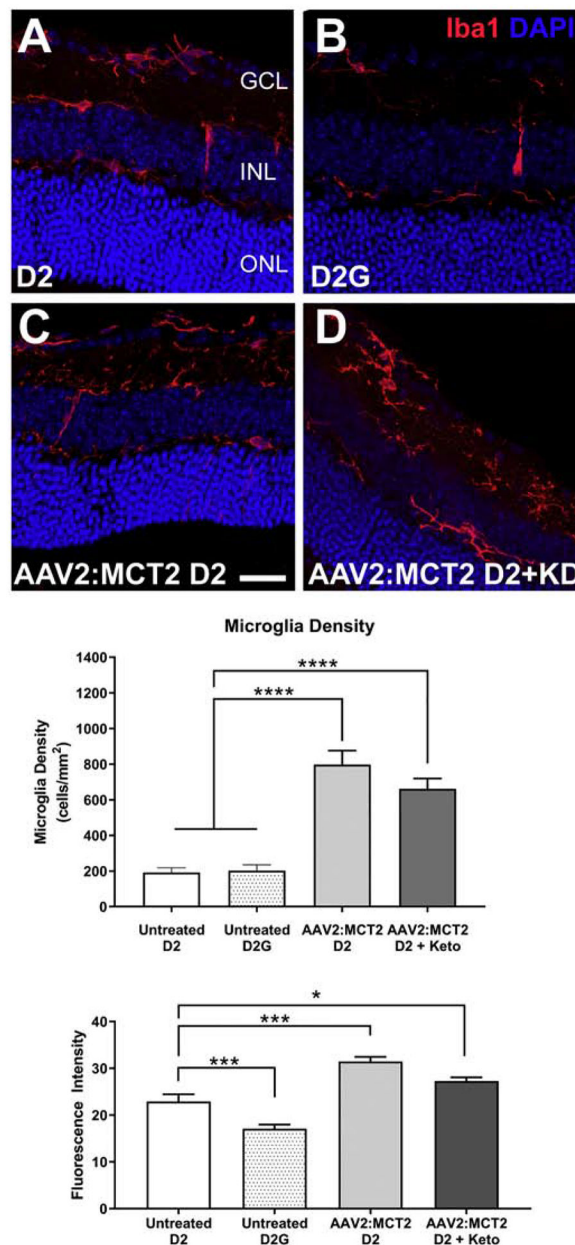
Figure 5:

Iba1 fluorescence and microglia density in peripheral retina from D2 mice injected with AAV2:MCT2. **A-D**. Photomicrographs showing the expression of Iba1 (red) in microglia by immunolabeling in retinas from D2 (**A**), D2G (**B**), D2 injected with AAV2:MCT2 (**C**), and D2 injected with AAV2:MCT2 mice on the ketogenic diet (KD) (**D**). Scale bar = 35μm. DAPI nuclear stain in blue. **E**. D2 mice injected with AAV2:MCT2 with or without ketogenic diet showed significantly higher microglia density than untreated D2 and D2G mice (p<0.0001); n=6 retinas per group and 2–3 sections per retina. Microglia were quantified at least 200μm from the optic nerve head. **F**. Untreated D2 mice had significantly higher Iba1 fluorescence than untreated D2G mice (p<0.001), but significantly lower Iba1 fluorescence than either AAV2:MCT2 injected D2 mice (p<0.001) or AAV2:MCT2 injected
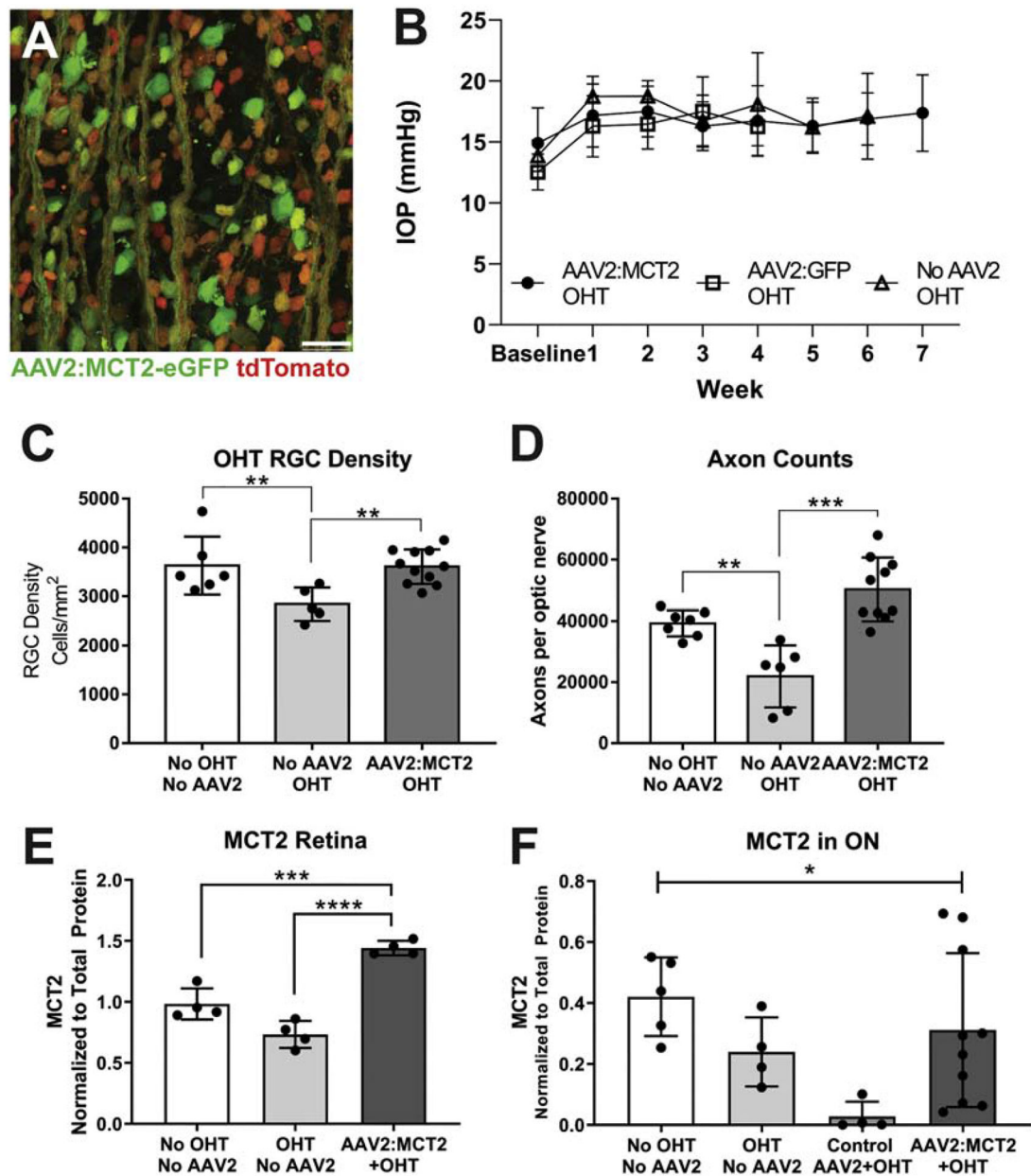
D2 mice on the ketogenic diet (p<0.05); an average of 30 sections were analyzed per group. Error bars are SEM.

Figure 6:

Retinal ganglion cell (RGC) and optic nerve (ON) axon integrity, and MCT2 protein levels in mice after ocular hypertension (OHT). **A**. Photomicrograph of AAV2:MCT2 infection in flatmount retina without OHT; AAV2:MCT2 virus infection reporter is eGFP (green), and RGC-specific label RBPMS (red). Scale bar = 50μm. **B**. Intraocular pressure (IOP) elevation in the three OHT experimental groups. Each OHT group IOP was significantly increased over baseline, $p<0.0001$, though not statistically different from each other. Error bars are SEM. **C**. RGC density is significantly increased by AAV2:MCT2 injection after OHT (n=11) compared to OHT alone (n=5; $p<0.01$). OHT alone resulted in significant RGC loss compared to control (no OHT and no AAV2, n=6; $p<0.01$). **D**. Axon number in the ON of OHT mice (n=6) is significantly decreased compared to control (No OHT, n=6; $p<0.001$),

then rescued by injection with AAV2:MCT2 after OHT (n=10; p<0.001). **E.** MCT2 protein in retina is significantly higher in the OHT group injected with AAV2:MCT2 (n=4) compared to both control (No OHT, n=4; p<0.001) and OHT alone (n=4; p<0.0001). **F.** MCT2 protein in ON is significantly different across groups by one-way ANOVA (p<0.05); n=5 for control (No OHT, No AAV2), n=4 for OHT, n=4 for OHT + Control AAV2, and n=10 for AAV2:MCT2 + OHT. Error bars are SD.
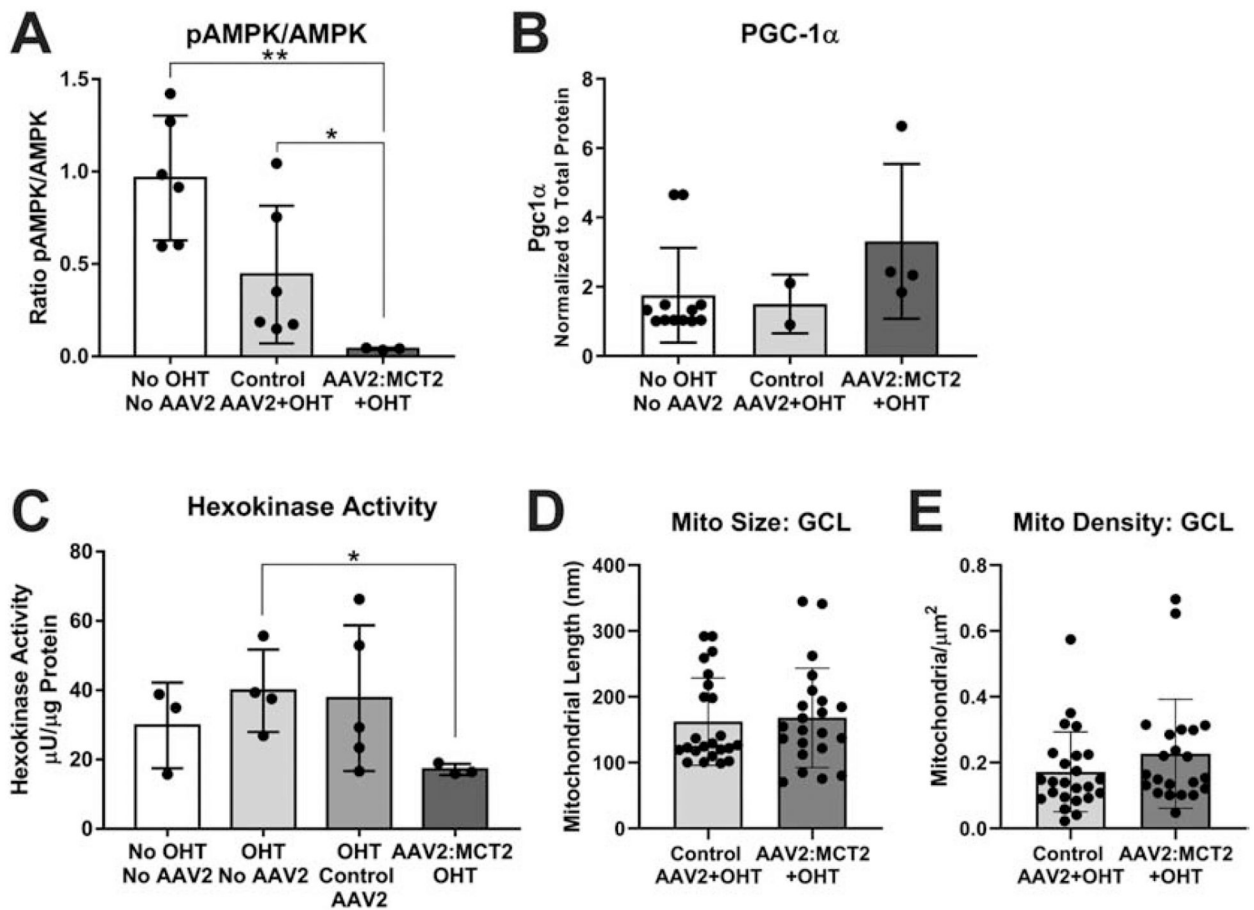
Figure 7:
Metabolic changes in ON from OHT mice injected with AAV2:MCT2. **A**. The ratio of phosphorylated AMP kinase (pAMPK) to AMPK is significantly lower in OHT mice injected with AAV2:MCT2 (n=5) compared to control mice (no OHT or virus, n=6) and OHT mice injected with AAV2:GFP (n=6; p<0.01, p<0.05 respectively). **B**. PGC-1α protein in ON did not differ statistically across groups. ON sample number was n=12 for the No OHT, No AAV2 group, n=3 for the Control AAV+MCT2 group, and n=4 for the AAV2:MCT2+OHT group. **C**. Hexokinase activity is significantly decreased in OHT mice injected with AAV2:MCT2 (n=3) compared to OHT mice alone (n=4; p<0.05). ON sample number was n=3 for the No OHT, No AAV2 group, and n=5 for the OHT Control AAV2 group. **D**. Mitochondria size and **E**. Mitochondria density in the ganglion cell layer (GCL) did not differ across the Control AAV2+OHT (n=24 retinal sections across 3 mice) and AAV2:MCT2+OHT (n=22 retinal sections across 3 mice) groups. Error bars are SD.
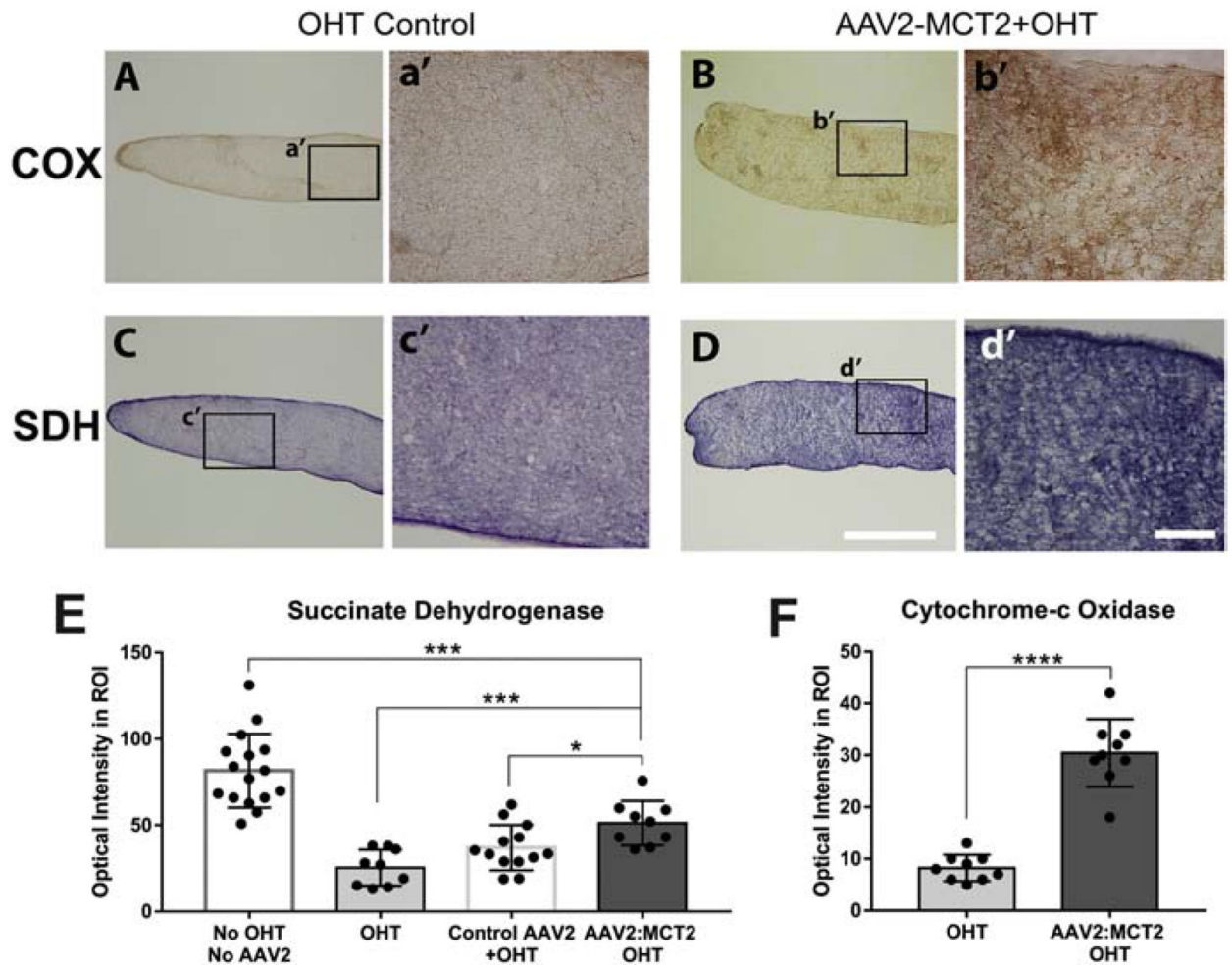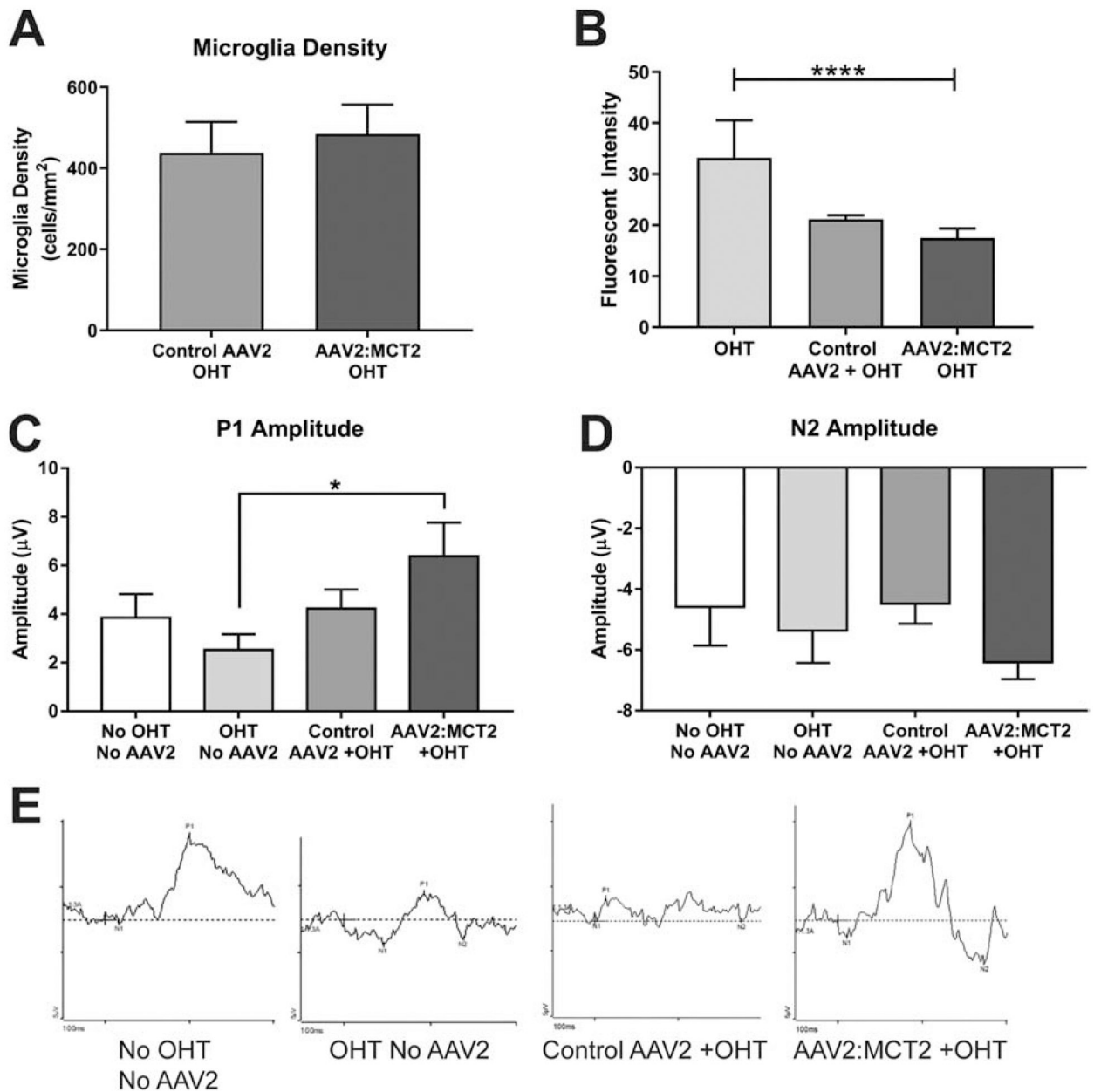
Figure 8:
Cytochrome-c oxidase (COX) and succinate dehydrogenase (SDH) activity in OHT optic nerves. **A-B**. COX histochemistry in OHT mouse ON (**A**), and OHT with AAV2:MCT2 injection (**B**). Higher magnification insets of OHT control (**a'**) and AAV2:MCT2 + OHT (**b'**) show greater DAB intensity after OHT with AAV2:MCT2. Quantification of histochemistry is shown in F. Scale bar=100μm. **C-D**. SDH histochemistry in OHT mouse ON (**C**) and OHT with AAV2:MCT2 injection (**D**). Scale bar=1000μm. Higher magnification insets of OHT control (**c'**) and AAV2:MCT2 + OHT (**d'**) indicate greater nitroblue tetrazolium intensity after OHT with AAV2:MCT2. **E**. SDH activity is significantly higher in AAV2:MCT2 with OHT ON (n=9 sections across 3 mice) compared to both OHT alone (n=9 sections across 3 mice), and OHT ON injected with control AAV2 (AAV2:GFP) (n=13 sections across 3 mice; p<0.001 and p<0.05, respectively). SDH activity is significantly lower in OHT animals injected with AAV2:MCT2 than in control mice (no OHT or AAV2, n=16 sections across 3 mice). **F**. COX activity is significantly higher in OHT mouse ON injected with AAV2:MCT2 (n=9 sections across 3 mice) compared to OHT alone (n=9 sections across 3 mice; p<0.0001). Error bars are SD.

Figure 9:
Retinal microglia and pattern electroretinogram in OHT mice. **A**. Microglia density did not differ between OHT eyes injected with control virus (AAV2:eGFP, n=12 sections from 3 retinas) or AAV2:MCT2 (n=16 sections from 4 retinas). **B**. Intensity of Iba1 immunolabeling was significantly different across groups, with virus injection having a lowering effect on fluorescence intensity of Iba1 (ANOVA, p<0.0001). Samples sizes for this analysis was n=12 retinal sections from 3 retinas per group. **C**. Pattern electroretinogram shows significantly higher P1 amplitude in OHT animals injected with AAV2:MCT2 (n=12 mice) than in OHT alone (n=12 mice; p<0.05). Sample size also n=12 for the No OHT, No AAV2; and the Control AAV2+OHT groups. **D**. N2 amplitude did not differ across

experimental groups; sample number as in **C**. Error bars are SD. **E**. Example PERG traces for each of the groups represented in **C** and **D**.

Table 1.

Indices for DBA/2J Mice on the Ketogenic or Control Diets

	Baseline IOP (mmHg)	Terminal IOP (mmHg)	Baseline Weight (g)	Terminal Weight (g)	Food Intake by Week (g)	kCal by Week	Plasma β-HB (mM)	Blood Sugar (mg/dL)
AAV2:MCT2 D2 Keto	16.8 ± 0.8	21.2 ± 0.9	29.7 ± 1.0	36.8 ± 1.4	12.9 ± 0.8	87.4 ± 5.9	0.753 ± 0.104	113.6 ± 6.6
AAV2:MCT2 D2 Control	17.1 ± 0.6	21.0 ± 0.7	30.2 ± 0.8	31.1 ± 0.8	20.1 ± 0.5	78.8 ± 2.0	0.062 ± 0.017	103.7 ± 6.3

±SEM; β-HB=β-hydroxybutyrate

Table 2.

Antibodies Used

Antibody	Dilution	Compa ny	Host
AMPK α 1 2B7	1:100 for Wes	Novus Biologicals	α-Mo
GFAP	1:500 for IF	Abcam	α-Gt
Iba1	1:300 for IF	Wako	α-Rb
MCT1	1:25 for Wes	Santa Cruz Biotechnology	α-Mo
MCT2	1:250 for IF	Frontier Institute	α-Rb
MCT2	1:25 for Wes	Bioss	α-Rb
NeuN	1:250 for IF	Millipore	α-Mo
pAMPK (Thr 172)	1:50 for Wes	Novus Biologicals	α-Rb
PGC-1α	1:50 for Wes	Novus Biologicals	α-Rb
RBPMS	1:200 for IF	Cell Signaling	α-Rb
Tom20	1:100 for IF	Santa Cruz Biotechnology	α-Gt

Wes=Protein Simple Wes capillary electrophoresis instrument